COVER SHEET

Spectroscopic characterization of Mn-rich tourmalines

B. Jagannadha Reddy, Ray L. Frost•, Wayde N. Martens, Daria L. Wain and J. Theo Kloprogge

Inorganic Materials Research Program, Queensland University of Technology, 2 George Street, Brisbane, GPO Box 2434, Queensland 4001, Australia.

Abstract:

Electronic and vibrational spectra of two different tourmalines: green and pink coloured minerals from Minas Gerais, Brazil have been investigated by UV-visible, NIR, IR and Raman spectroscopy. The behaviour of transition metal ions in their electronic spectra is presented. Both minerals show a strong broad band at ~300 nm (33300 cm^{-1}) due to Mn(II) ion. In pink tourmaline three sharp bands at 365, 345, and 295 nm (27400, 28990 and 33900 cm^{-1}) are assigned to $^{6}A_{1g}(S) \rightarrow {}^{4}T_{2g}(D)$, $^{6}A_{1g}(S) \rightarrow {}^{4}E_{g}(D)$ and $^{6}A_{1g}(S) \rightarrow {}^{4}T_{1g}(F)$ transitions of Mn(II) ion. The pink colour arises from Mn(II) ion while the band at 520 nm comes from Mn(III) ion which acts as an aid to the transmission window from 700-to-900 nm in pink tourmaline. NIR spectroscopy provides evidence for Fe(II) through the observation of two bands at

• Author to whom correspondence should be addressed (r.frost@qut.edu.au)
P: +61 7 3864 2407 F: +61 7 3864 1804

10240 and 8000 cm^{-1}. The observation of four OH stretching bands in the hydroxyl stretching region 3800 to 3200 cm^{-1} near 3650, 3600 and 3555 and 3460 cm^{-1} shows mixed occupancy of octahedral sites in the minerals studied. The band positions in the spectra of green and pink tourmalines differ slightly due to variations in composition. Experimentally, a number of cation-oxygen vibrational modes in the Raman spectra could be observed in the low wavenumber region 1200-to-200cm^{-1}.

Keywords: XPS; UV-Vis and NIR spectroscopy; Tourmaline; Mn(II) octahedral symmetry; Overtone and combination bands; Vibrational spectroscopy.

1. Introduction

Tourmalines are important petrogenetic indicators since a number of chemical elements can be incorporated in them by partial and or complete substitution depending on the mineralogical and metallogenic history of the rock [1-4]. The spectra of green and blue tourmalines are dominated by pleochroic absorption bands around 700 (14000 cm^{-1}) and 1100 nm (9000 cm^{-1}) where as the pink tourmalines exhibit different spectra from those of green / blue samples [5]. Transition metal cations like Fe and Mn in different valence states incorporated basically in Y-sites in the tourmaline structure.

Tourmaline has a very complex chemical composition with space group, R3m – C_{3v}^5. It can be represented by the general formula XY_3Z_6 $(Si_6O_{18})(BO_3)_3W4$, where X = Na^+, Ca^{2+}, K^+); Y = Mg^{2+}, vacancy ($^{2+}$, Fe^{2+}, Mn^{2+}, Al^{3+}, Fe^{3+}, Mn^{3+}, Cr^{3+}, Li^+; Z = Al^{3+}, Mg^{2+}, Fe^{3+}, Cr^{3+}, V^{3+}, and W = O^{2-}, OH^-, F^-, Cl. The structure consists of corner-shared tetrahedra forming hexagonal rings which are principally occupied by Si [6]. Boron is in triangular coordination and has no known substitutions [7]. There are two types of octahedra; the Y octahedra and the slightly smaller, distorted Z octahedra. The Y and Z octahedra share edges to form brucite-like fragments [8,9]. OH groups occupy two structurally distinct positions: the centre of the hexagonal rings and the corner of the brucite-like fragments of three edge-sharing octahedra [10].

Mn-rich tourmalines have been extensively investigated and the results are focussed mainly on composition and geological environments [11,12]. Burns et al. [9]

described crystal structure of a number of Mn-rich tourmalines whose composition varies from 0.35 to 6.23 wt % MnO. Hawthorne and Henry [13] reviewed crystal-chemical aspects of substitutions including lighter elements and structural features in tourmaline. The crystal chemistry of tourmalines was studied by Camera et al. [14] using the combination of SREF, EPMA, and SIMS and explained the difficulties in determining lighter elements with high accuracy in tourmalines. Such elements in tourmalines are crucial to the further understanding of chemical substitutions and order-disorder schemes. A recent study of crystal chemistry and optical spectra of Mn-rich tourmaline from Austria revealed the compositions of MnO and FeO ~ 8.5 and 0.15 wt % respectively [15] and its optical absorption spectra were attributed to Mn^{3+}, and Mn^{2+}in the visible region where as near infrared cited to ferrous ion with no assignment of the bands. Gasharova et al. [16] reported Raman spectroscopy of different tourmalines in the low wavenumber region (spectral range 1500-150 cm^{-1}) where in the spectra differ in intensity from each other studied, due to the different optical parameters.

This paper reports the electronic and vibrational spectra of two different tourmalines; green and pink coloured minerals from Minas Gerais, Brazil. We demonstrate the behaviour of transition metal ions in their electronic spectra. The properties of the minerals observed in the IR spectra are discussed. OH stretching bands are high lighted here since they are very sensitive to crystal structural changes. Raman spectroscopy displays a number of bands in the low wavenumber region, 1200-200 cm^{-1}, due to cation-oxygen vibrational modes.

2. Analytical methods

2.1. Sample preparation

Two samples (green and pink minerals) belonging to tourmaline group were selected for the present study, originally from the collection of the Department of Geosciences, Texas Tech. University, and these samples originated from Minas Gerais, Brazil. They were analysed by an electron probe using energy dispersive X ray analysis and XPS techniques for chemical composition. Fragments of each ~ 1mm^2 were employed for the study of Raman and IR spectroscopy. The powdered minerals were used for the electronic spectra by reflectance spectroscopy in the UV-Vis region and for powdered XPS.

2.2. XPS analysis

Data was acquired using a Kratos Axis ULTRA X-ray Photoelectron Spectrometer incorporating a 165 mm hemispherical electron energy analyser. The incident radiation was monochromatic Al X-rays (1486.6 eV) at 225 W (15 kV, 15 ma). Survey (wide) scans were taken at analyser pass energy of 160 eV and multiplex (narrow) higher resolution scans at 80 eV. Survey scans were carried out over 1200-0 eV binding energy range with 1.0 eV steps and a dwell time of 100ms. Narrow higher resolution scans were run with 0.1 eV steps and 250 ms dwell time. Base pressure in the analysis chamber was 1.0×10^{-9} torr and during sample analysis it was maintained as 1.0×10^{-8} torr. Atomic concentrations were calculated using the Kratos Vision 2 software and a linear baseline. Due to interference to the Mn 2p1/2 peak, only the Mn 2p3/2 was used with a reduction of 2/3 in the elemental sensitivity factor.

2.3. UV-Vis spectroscopy

The UV-Vis spectroscopy is an ideal tool for study of coloured minerals, containing transitions metals. Spectra of d-d transitions mainly fall in this region and can be studied either by absorption or by reflection. The technique of reflectance spectroscopy is most suitable for minerals including dark coloured and or non-transparent materials. Varian Cary 3 UV-Visible spectrophotometer, equipped with Diffuse Reflectance Accessory (DRA) was employed to record the electronic spectra of the samples in the region between 200 and 900 nm. This technique allows the study of the reflectance spectra of the samples in the powder form. The DRA consists of a 73 mm diameter integrating sphere, featuring an inbuilt high performance photomultiplier. Sample was mounted on coarse filter paper (# 1), by resuspending the sample and submerging the filter paper into the suspension. Initially a base line was recorded using two pressed polytetrafluoroethylene (PTFE) as reference disks. Next, the sample was mounted flat over the sample port and the reflectance spectrum of the sample, relative to the reference disks, was collected by the integrating sphere. By placing the sample flat any specular components, of reflectance, should be directed out of the DRA entrance port, as the angle of incidence is 0^0. The diffuse reflectance measurements were converted into absorption (arbitrary units) using the Kubelka-Munk function ($f(R_\infty) = (1- R_\infty)^2/2R_\infty$). Data manipulation was performed using Microsoft Excel.

2.4. Infrared and near-infrared spectroscopy (NIR)

Infrared spectrum was obtained using a Nicolet Nexus 870 FTIR spectrometer with a Smart Endurance single bounce diamond ATR cell. The technique is a

reflectance method using powdered films or small crystals. The spectrum was obtained over the 4000-550 cm^{-1} region by the co-addition of 64 scans with a resolution of 4 cm^{-1} and a mirror velocity of 0.6329 cm/s. The lower limit of the diamond ATR cell is 550 cm^{-1} as below this wavenumber the diamond absorbs all the infrared radiation. The spectrum was obtained over the 4000-550 cm^{-1} region by the co-addition of 64 scans with a resolution of 4 cm^{-1} and a mirror velocity of 0.6329 cm/s.

NIR spectrum was collected on a Nicolet Nexus FT-IR spectrometer fitted with a Nicolet Near-IR Fibreport accessory. A white light source was employed with a quartz beam splitter and TEC NIR InGaAs detector. The near infrared spectrum was obtained from 11000 to 4000 cm^{-1} by the co-addition of 64 scans at the resolution of 8 cm^{-1}. A mirror velocity of 1.2659 m/s was used. The spectra were transformed using the Kubelka-Munk algorithm for comparison with that of absorption spectra. Spectral manipulations such as baseline adjustment, smoothing and normalisation were performed using the Spectracalc software package GRAMS (Galactic Industries Corporation, NH, USA).

Band component analysis was undertaken using the Jandel 'peakfit' software package which enabled the type of fitting function to be selected and allows specific parameters to be fixed or varied accordingly. Band fitting was undertaken using a Lorentz-Gauss cross-product function with the minimum number of component bands used for the fitting process. The Gauss-Lorentz ratio was maintained at values greater than 0.7 and fitting was undertaken until reproducible results were obtained with squared correlations of r^2 greater than 0.995.

2.5. Raman microprobe spectroscopy

A small crystal of about 1mm^2 was fixed and oriented on the stage of an Olympus BHSM microscope, equipped with 10x and 50x objectives and part of a Renishaw 1000 Raman microscope system, which also includes a monochromator, a filter system and a Charge coupled Device (CCD). Raman spectra were excited by a HeNe laser (633 nm) at a resolution of 2 cm^{-1} in the range; 4000-100 cm^{-1}. Repeated acquisition using the highest magnification was accumulated to improve the signal to noise ratio. Spectra were calibrated using the 520.5 cm^{-1} line of silicon wafer. In order to ensure that the correct spectra are obtained, the incident excitation light was scrambled. Details of the experimental technique have already been reported [17-19].

3. Results and discussions

3.1. XPS analysis of tourmaline

Tourmaline has very complex chemical composition and it is difficult to determine the accurate composition completely [14]. In this work only qualitative analysis has been undertaken. Therefore, XPS analyses were performed to check the elemental composition in these two minerals. Under wide scan (PE = 160 eV and 1 eV steps), major elements were detected. But minor elements which are weak in intensity could be detected in higher resolution only (PE = 80 eV and 0.1 eV steps). The narrow scans of Al 2p (reference), Na 2s, Li 1s, Mn 2p, Fe 2p andB1s were run to analyse minor composition. The composition of the two tourmaline samples show Si and Al as major while Boron is also present but its concentration appears to be less than Al and Si. In our study under minor composition, it is found that Mn and Fe are

present in green sample but Li below detection limit where as in pink sample has Mn and Li but and Fe is below detection limit. Traces of Ca and Mg are present in both the minerals. Considerable levels of peaks observed in the XPS spectrum for K and Zn indicate that these two elements are present as impurity inclusions in green and pink tourmalines respectively.

3.2. UV-Vis and NIR spectroscopy

Electronic spectra may be obtained by using a combination of UV-visible and NIR spectroscopy. Figs. 1a and 1b represent the electronic spectra of tourmalines. Both the samples show a significant feature near 400 nm that arises from dd transitions of divalent manganese. Three bands are observed in green tourmaline; one weak band at 715 nm (14000 cm^{-1}), a well defined band at 320 nm (31250 cm^{-1}) and strong absorption with an edge extended as a tail to extreme UV limit, 200 nm (5000 cm^{-1}). The band in the visible spectrum at 715 nm implies intervalence charge transfer (IVCT) through an electron transfer between Fe(II) –Fe(III) ions. A similar observation has been made by Faye et al. [5] in blue and green tourmalines and explained that at an electron transfer is induced from Fe(II) ions in (Fe, Mg) sites to Fe(III) ions in the adjacent sites of Al and/or (Fe, Mg). The broad band in UV region with shoulders on either side and a weak band at 520 nm (19230 cm^{-1}) are the characteristics of Mn ions in pink tourmaline (Fig. 1b).Two narrow bands near 415 nm assigned to Mn(II) and one strong band in the visible region at 520 nm is assigned to Mn(III) in Mn-rich tourmaline from Austria [20]. In the spectrum of pink tourmaline (Fig. 1b), the band at 520 nm is due to Mn(III) ions in the high spin state, S = 2 in weakly, distorted octahedral sites [21]. The broad band resolved into three

sharp bands from Gaussian analysis are identified as Mn(II) octahedral bands. Such sharp bands were observed in manganese bearing silicates pyroxmangite, rhodonite, bustamite, and serandite and the bands at 27700 and 29100 cm^{-1} are attributed to the $^6A_{1g}$ (S) to $^4T_{2g}$ (D) and ^4E_g (D) transitions [22]. In the preset work, the two bands at 365 and 345 nm (27400 and 28990 cm^{-1}) are identified as to $^6A_{1g}$(S) $\rightarrow$ $^4T_{2g}$ (D) and $^6A_{1g}$ (S) $\rightarrow$ ^4E_g (D) transitions of Mn(II) in octahedral sites. The third band at 295 nm (33900 cm^{-1}) is assigned to $^6A_{1g}$ (S) $\rightarrow$ $^4T_1$g (F) from Tanabe and Sugano diagram drawn for d^5 configuration [23].

The near-IR spectra of the two minerals are shown in Fig. 2. Bands in the 7700-6500 cm^{-1} region (Fig. 2b) are attributed to the first fundamental overtone of the hydroxyl stretching modes. Combination of the stretching and bending modes of MOH are analysed in the 4800-4000 cm^{-1}(Fig. 2c). A strong broad band appears in the range 10400-7900 cm^{-1} for all ferrous ion complexes [24]. These bands are very weak due to low concentration of iron and hence their intensities are magnified by 1200 (I) to see the broad band structure. The main band for green tourmaline (Fig. 2a) at 10240 cm^{-1} with a split component at 8000 cm^{-1} is assigned to the $^5T_{2g}$ $\rightarrow$ ^5E_g transition. The average of these bands gives the value of 10Dq (9120 cm^{-1}) [25]. The separation of the two bands of the order of 2200 cm^{-1} confirms distorted octahedral Fe(II) sites in the tourmaline minerals [26,27].

The feature observed at 7600 cm^{-1} might be due to the combination of the overtone of OH1 stretch (observed in IR at 3655 cm^{-1}) and MgOH bending mode (IR band at 1100cm^{-1}) [3655x2 + 1100 = 8410 cm^{-1}]. Two bands at ~7000 and 6500 cm^{-1} are strong and assigned to the first overtone of OH3 groups of IR bands appearing at

~3600 and near 3460 cm^{-1} (Fig. 3a). Tourmaline is structurally and chemically complex borosilicate mineral with the general formula $XY_3Z_6(Si_6O_{18})(BO_3)_3(OH,F)_3(OH,F)$ where X-sites are normally Na and Ca, or Mg, Fe or Mn. The Z and Y sites are generally occupied by Al. However, in ideal elbaite only 50 % of the Y sites are occupied by Al and the other 50 % of the Y site are occupied by Li. Only in olenite both Y and Z sites are generally occupied by Al. A number of vibrational bands are observed in the 4800-4000 cm^{-1} (Fig. 2c). A group of sharp bands centred near 4500 and 4300 cm^{-1} is remarkably differing from hydroxyl bands and these are concerned with stretching and bending modes of M-OH in tourmaline [28]. The band at ~4600 cm^{-1} is due to combination bands involving Al-OH. The sharp bands near 4500 and 4300 cm^{-1} are due to Mg(OH) and Fe(OH) since a large number of metallic elements are in Y sites of tourmaline. Sharp bands located around 4500 and 4300 cm^{-1} are compared with the spectra of schorl and dravite in which Fe and Mg respectively prevail in Y site and are ascertained to Mg-OH stretch near 4500 cm^{-1} and the lowest frequency group bands near 4300 cm^{-1} to Fe-OH units. It is probable that these bands originate from the combination of the hydroxyl stretching and hydroxyl bending modes of a particular MOH unit (i.e. 3580 + 1100 = 4680 cm^{-1}).

3.3. Infrared spectroscopy

For tourmalines, the OH groups (OH1 and OH3) are distributed into two different sites: Y and Z cation sites. Two types of behaviour were reported; in elbaite-schorl series; three O-H bands in Fe-rich elbaites and four O-H stretching bands for Li-bearing schorl [29]. The spectra of the hydroxyl stretching region for the present

samples are shown in Fig. 3a. In the present study, four bands derived from green and pink tourmalines are due to the mixed occupancy of octahedral sites where a number of local normal vibrations exists. The strongest band of O-H stretching vibrations at 3460 cm^{-1} in pink tourmaline can be connected only with prevailing octahedral cation. It can be only Al in the Y site, because this

pink tourmaline corresponds to olenite by composition and this band is strongest in the IR spectrum of olenite (3800-3200 cm^{-1} range). The band in the range 3560-3500 cm^{-1} is the typical for schorl and dravite . For this reason, the weak narrow band near 3555 cm^{-1} can be due to the local vibrations OH groups connected with Al in Z sites and Fe, Mn or Mg in Y sites .The band positions and their assignments are presented in Table 1 and compared with the bands reported for Fe green tourmaline and Li-schorl from northeast Minas Gerais state, Brazil [30]. Band positions of green tourmaline are higher than that of pink tourmaline. Thus pink tourmaline bands are sharp and are shifted to the lower wavenumbers. Broadening of the bands and splitting of the ν_2 mode by appearance of a component at 3555 cm^{-1} in green tourmaline resulted in iron(II) impurity. Cation replacements that involve a valency change modify anion vibrations, and cause shifts in band frequencies in tourmalines [10]. The occurrence of bands in low wavenumber region 1500-to-800 cm^{-1} is shown in Fig. 3b and their assignments are presented in Table 1. Two bands around 1300 cm^{-1} are identified as BO_3 groups [31] and the strong bands near 1000 cm^{-1} are related to stretching vibrations of the Si_6O_{18} rings. The band at 1100 cm^{-1} as a shoulder on the higher wavenumber side of the band near 1000 cm^{-1} is attributed to MgOH bending modes.

3.4. Raman spectroscopy

The study of Raman spectra of green and pink tourmalines in the low wavenumber range 1200-to-200 cm^{-1} is represented in Figs. 4a & b. The vibrational types are calculated by Mihailova et al. [32,33]. Due to the different optical parameters of the tourmalines, their Raman spectra differ in intensity from each other. There are four main Raman groups of bands centred at ~ 1100, 700, 400 and 250 cm^{-1} and their assignments are given in Table 2 along with a selected tourmalines studied by Gasharova et al. [16]. There is a close relationship between the data of elbaite type reported and the present study of green and pink tourmalines, since they belong to the same series of tourmalines. The first group of broad bands arise from Si-O stretching, the second from B-O stretching, bending modes of O-B-O and B-O-Al and symmetrical Si-O-Si deformations. The sharp peak with marked intensity at 375 cm^{-1} in both the spectra of the samples implies strong bonding of Al-O. The lowest wavenumber band at 225 cm^{-1} originates from Mg-O and a shoulder of this band at 250 cm^{-1} on higher wavenumber side represents O-Al-O bending mode. The effect of Fe impurity is seen on this band in green tourmaline (Figs.4a & b) and its intensity is depleted. The same band is resolved in pink tourmaline into three sharp peaks at 275, 250 and 225 cm^{-1} and further confirms Mn-O vibrational mode more clearly, at 77K (Fig. 4a). This feature mainly differentiates between green and pink tourmalines.

4. Conclusions

UV-Vis spectroscopy plays a key role to display distinction between green and pink tourmalines. A significant feature appears at ~300 nm (33300 cm^{-1}) in both samples due to dd transitions of divalent manganese. The absorption band at 715 nm (14000

cm^{-1}) in green tourmaline is a strong indication of Intervalence charge transfer (IVCT) that takes place between $Fe^{2+} \leftrightarrow Fe^{3+}$. Pink tourmaline exhibits a typical absorption spectrum due to manganese impurity and is characterized by three sharp bands in UV region due to Mn(II) ion and one broad band in the visible spectrum arises from Mn(III) ions in the high spin state, S = 2 in weakly, distorted octahedral sites. It is shown that IR and Raman spectra can be taken as a base to classify the tourmaline minerals. The bands in O-H stretching region 3800-to-3200 cm^{-1} serve as a best indicator to distinguish between the two groups. The existence of similarity is evident from IR and Raman spectra of the studied samples since both the minerals belong to the same series of tourmalines.

Acknowledgements

The financial and infra-structure support of the Queensland University of Technology QUT), Inorganic Materials Research Program is gratefully acknowledged. We thank the Australian Research council (ARC) for funding the facilities used in this research work. On of us, B. J. Reddy is grateful to QUT for the award of Visiting Fellowship.

References

[1] D.B. Clarke, N.C. Reardon, A.K. Chatterjee, D.C. Gregoire, Econ. Geol. 54 (1989)1921.

[2] J.M. Cleland, G.B. Morey, P.L. McSwiggen, Econ. Geol. 91 (1996) 1282.

[3] W.L. Griffin, J.F. Slack, A.R. Ramsden, T.T. Win, C.G. Ryan, Econ. Geol. 91 (1996) 657.

[4] D.J. Henry, C.V. Guidotti, . Am. Mineral. 70 (1985) 1.

[5] G.H. Faye, P.G. Manning, E.H. Nickel, Am. Mineral. 53 (1968)1174.

[6] P.E. Roseberg, F.E. Foit, Am. Mineral. 64 (1979) 180.

[7] P. Povondra, Acta Universitatis Carolinae, Geologica 3 (1981) 223.

[8] J.D. Grice, T.S. Ercit, Neues Jahrb. Mineral. Abh. 165 (1993) 245

[9] P.C. Burns, D.J. MacDonald, F. Hawthorne, Can. Mineral. 32 (1994)31.

[10] C. T. Gonzalez, M. Fernandez, J. Sanz, Phys. Chem. Miner.15 (1988) 452.

[11] K. Schmetzer, H. Bank, N. Jb. Miner. Mh. Jg. 1884 (1984)61.

[12] G.R. Rossman, S.M. Mattson, Am. Mineral. 71 (1986) 599.

[13] F.C. Hawthorne, D.J. Henry, Eur. J. Mineral. 11 (1999) 201.

[14] F. Camara, L. Ottolini, F.C. Hawthorne, Am. Mineral. 87 (2002) 1437.

[15] A. Ertl, J.M. Hughes, S. Prowatke, G.R. Rossman, D. London, E.A. Fritz, Am. Mineral. 88 (2003) 1369.

[16] B. Gasharova, B. Mihailova, L. Konstantinov, Eur. J. Mineral. 9 (1997) 935.

[17] R.L. Frost, R.L. Weier, Thermochim. Acta 406 (2003) 221

[18] R.L. Frost, R.L. Weier, J.T. Kloprogge, J. Raman Spectrosc. 34 (2003) 760.

[19] R.L. Frost, R.L. Weier, Thermochim. Acta 409 (2004)79.

[20] I.L. Reinitz, G.R. Rossman, Am. Mineral. 73 (1998) 822.

[21] P.G. Manning, Can. Mineral. 11 (1973) 971.

[22] P.G. Manning, Can. Mineral. 9 (1968) 348.

[23] Y. Tanabe, S. Sugano, J. Phys. Soc. Japan 9 (1954) 753.

[24] R.G. Burns, Mineralogical Applications of Crystal Field Theory,
Ed., 2, Cambridge University Press, Cambridge, 1993.

[25] C.J. Ballhausen, Introduction to Ligand Field Theory, Mc-Graw Hill Book Company, New Delhi, 1962.

[26] A.V. Chandrasekhar, M. Venkataramanaiah, B.J. Reddy, Y.P. Reddy, R.V.S.S.N. Ravikumar, Spectrochim. Acta A 59 (2003) 2115.

[27] R.L. Frost, R.A. Wills, W. Martens, M. Weier, B. Jagannadha Reddy, Spectrochim. Acta A 62 (2005)42.

[28] R.L. Frost, O.B. Locos, H. Ruan, J.T. Kloprogge, Vib. Spectrosc. 27 (2001) 1.

[29] C. Castaneda, E.F. Oliveira, N. Gomes, A.C.P. Soares, Am. Mineral. 85 (2000) 1503.

[30] E.F. Oliveira, C. Castaneda, S.G. Eeckhout, M.M. Gilmar, R.R. Kwitko, E. De Grave, N.F. Botelho, Am. Mineral. 87 (2002) 1154.

[31] V.C. Farmer, The Infrared spectra of Minerals, Monograph 4, Mineralogical Society, 1974, p. 375.

[32] B. Mihailova, N. Zotov, M. Marinov, J. Nikolov, L. Konstantinov, J. Non-Cryst. Solids 167 (1994)265.

[33] B. Mihailova, B. Gasharova, L. Konstantinov, J. Raman Spectrosc. 27 (1996) 829.

.

Table 1. Assignments of the observed IR bands (cm^{-1}) for tourmalines and comparison with other tourmalines.

Mode	Fe-elbaite*	Assign.	Li-schorl*	Green tourmaline (present work)	Pink tourmaline (present work)	Assign.
ν_1	3641	OH1 $Li^{y}Al^{Y}Fe^{Y}$	3635	3655	3650	OH1 (Fe) $Al^{y}Fe^{Y}R^{Y}$
			3593	3625	3580	(OH1) (Li)$Li^{Y}Al^{Y}R^{Y}$
ν_2	3580	OH3 (Fe, Li, Al)$^{Y}Al^{Z}Al^{Z}$	3553	3590	3555	(OH3) (Fe,Mn,Mg)$^{Y}Al^{Z}$
				3555 c		(OH3) (Fe,Mn,Mg)$^{Y}Al^{Z}$
ν_3	3458	OH3 (Fe, Li, Al)$^{Y}Al^{Z}Al^{Z}$	3485	3475	3460	OH3 Al^{Y}
ν_4	-		-	1355	1360	BO_3 stretching vibration
ν_5	-		-	1300	1285	BO_3 stretching vibration
ν_6	-		-	1100	1110	MgOH bending
ν_7	-		-	1030	1027	Si_6O_{18} stretching vibration
ν_8	-		-	985	978	Si_6O_{18} stretching vibration
	-		-	930	875	Si_6O_{18} stretching vibration

* Oliveira et al. 2002; c – component

Table 2. Assignments of Raman frequencies (cm^{-1}) observed for tourmalines and comparison with other tourmalines.

Raman mode	*Buergerite-schorl (G1#)*	*Elbaite-type (G2#)*	*Dravite-buergerite-uvite (G3#)*	*Green tourmaline (Present work)*	*Pink tourmaline (Present work)*		*Type of modes**
					298K	*77K*	
ν_1	-	-	-	1175	1175	1170	δMgOH
ν_2	1056	1105	1050				Si-O_{br} str**
ν_3	1020	1059	1024	1085	1085	1090	Si-O_{non} Str
ν_4	969	989	973	1005	995	990	Si-O str
ν_5	777	760	753	-	-	-	Si-O str & Si-O-Si bend
ν_6	780	731	765	750	750	750	B-O str & O-B-O bend
ν_7	701	727	699	705	710	710	"breathing" of O_{br} in Si-O rings
ν_8	765	693	741	ov	ov	ov	B-O str B-O-Al bend
ν_9	674, 637	637	661, 640	635	640	642	Si-O_{br} rck
ν_{10}	437	508	481	510	540, 515	545, 515	Oxygen vibrations in Si-O rings
ν_{11}	403	407	409	410	410	410	O_{non}-Si-O_{non} bend
ν_{12}	369	373	365	375	375	375	Al-O str
ν_{13}	349	350	356	355, 320	350, 320	365, 320	Si-O_{non} rck
ν_{14}	-	-	-	275	275	275	Fe-O, Mn-O
ν_{15}	ov	244	ov	250	250	250	O-Al-O bend
ν_{16}	237	222	238, 215	225	225	225	Mg-O

Gasharova et al. 1997

* str: bond stretching; bend: bond bending; rck: bond rocking; ov: overlapped; -: Not observed

** O_{br}: bridging oxygens in the Si-O rings, which link two SiO_4 tetrahedra; O_{non}: non-bridging oxygens in the Si-O rings.

List of Figures

List of Tables

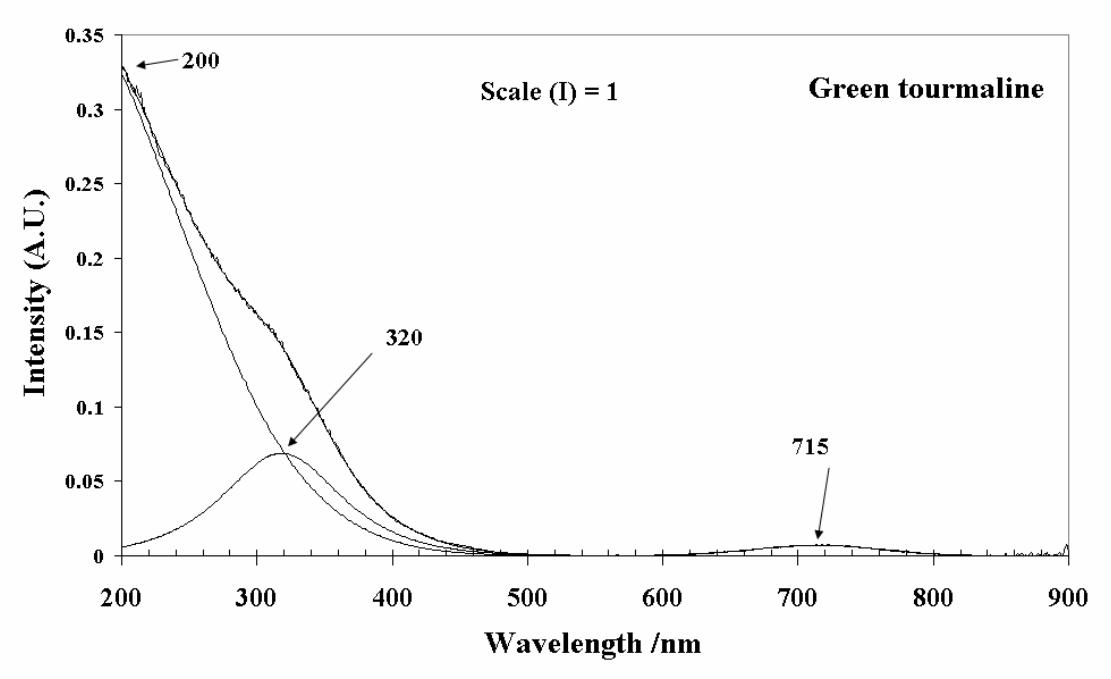
Green tourmaline
Scale (I) = 1
200
320
715
Intensity (A.U.)
Wavelength /nm
0.35
0.3
0.25
0.2
0.15
0.1
0.05
0
200
300
400
500
600
700
800
900

Fig. 1a

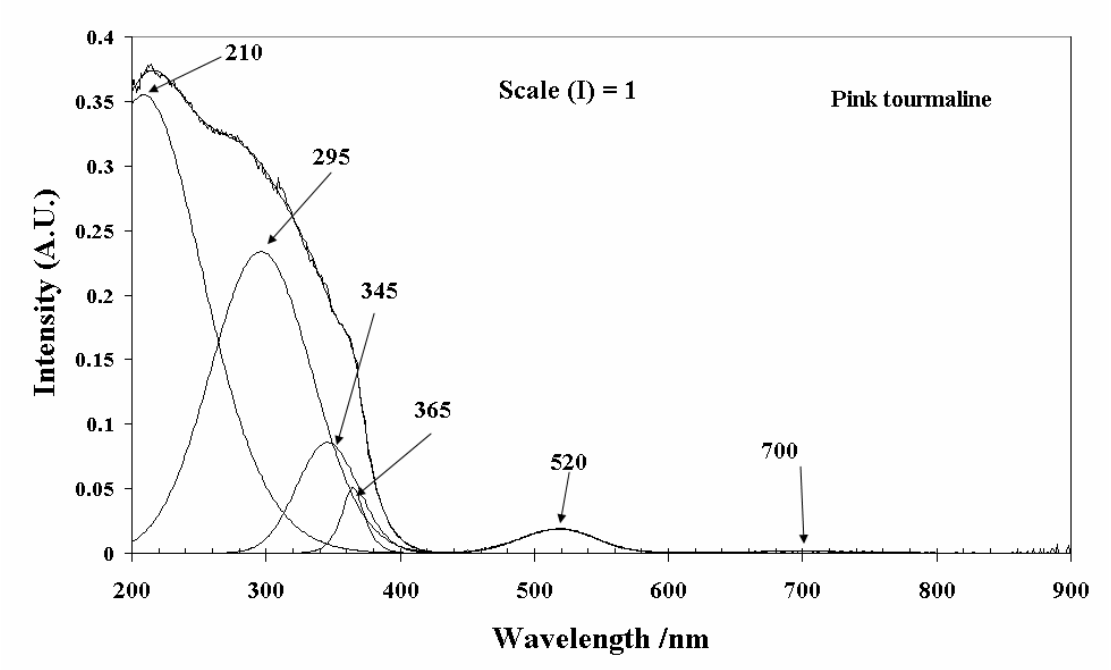
Pink tourmaline
Scale (I) = 1
210
295
345
365
520
700
Intensity (A.U.)
Wavelength /nm
0.4
0.35
0.3
0.25
0.2
0.15
0.1
0.05
0
200
300
400
500
600
700
800
900

Fig. 1b

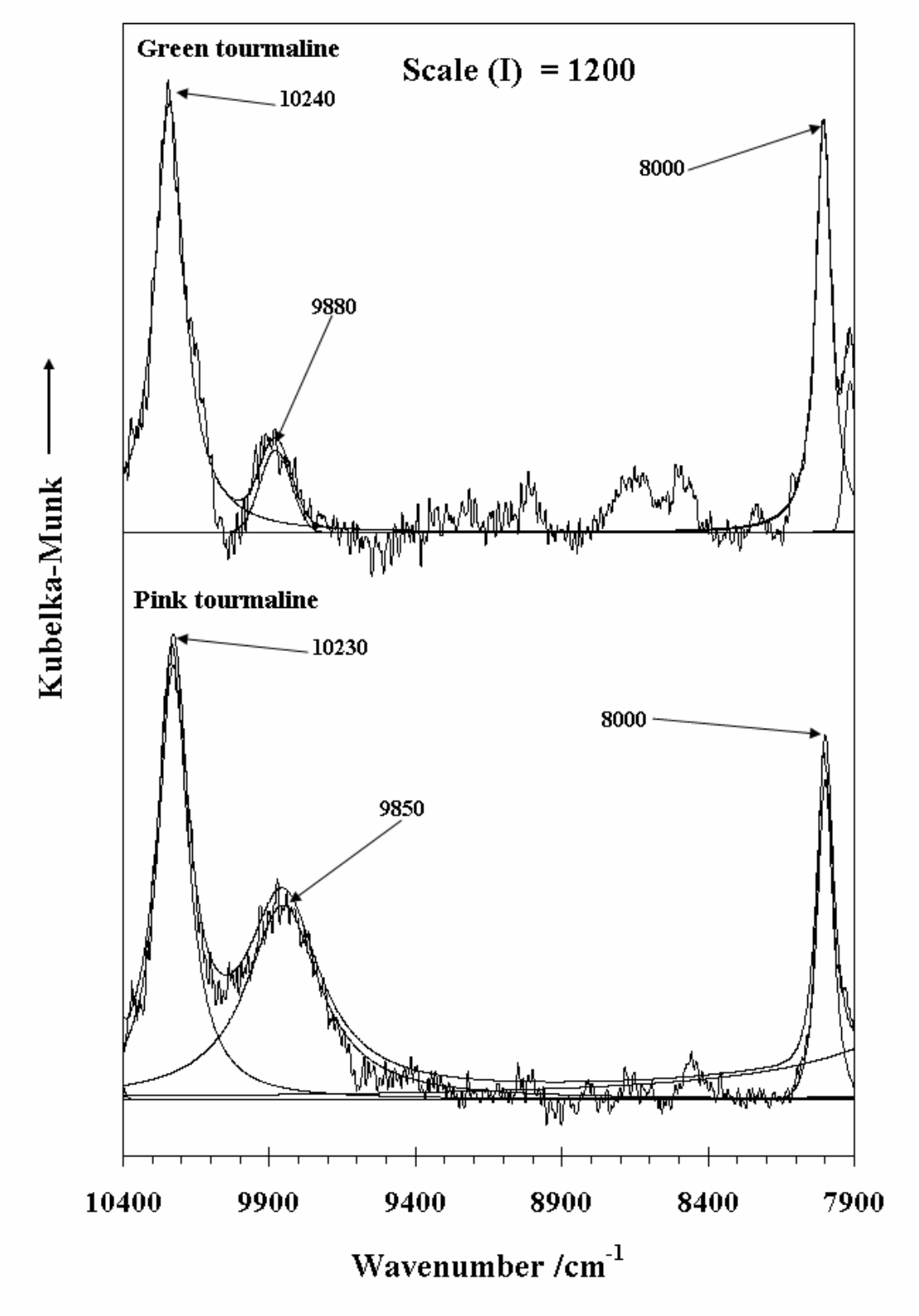
Green tourmaline
Scale (I) = 1200
10240
8000
9880
Pink tourmaline
10230
8000
9850
Kubelka-Munk
10400
9900
9400
8900
8400
7900
Wavenumber /cm-1

Fig. 2a

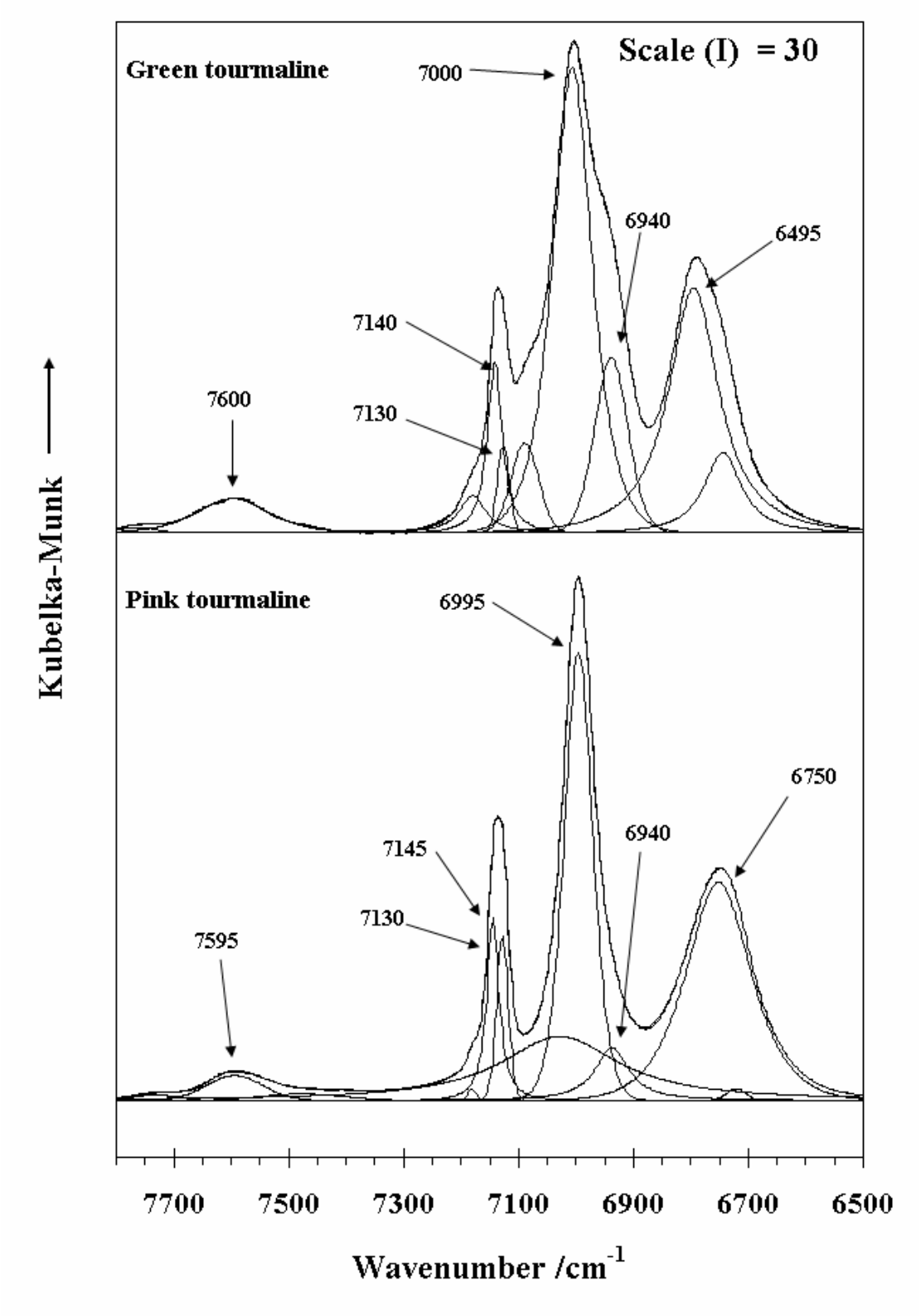
Green tourmaline
Scale (I) = 30
7000
6940
6495
7140
7600
7130
Pink tourmaline
6995
6750
7145
6940
7130
7595
Kubelka-Munk
7700
7500
7300
7100
6900
6700
6500
Wavenumber /cm-1

Fig. 2b

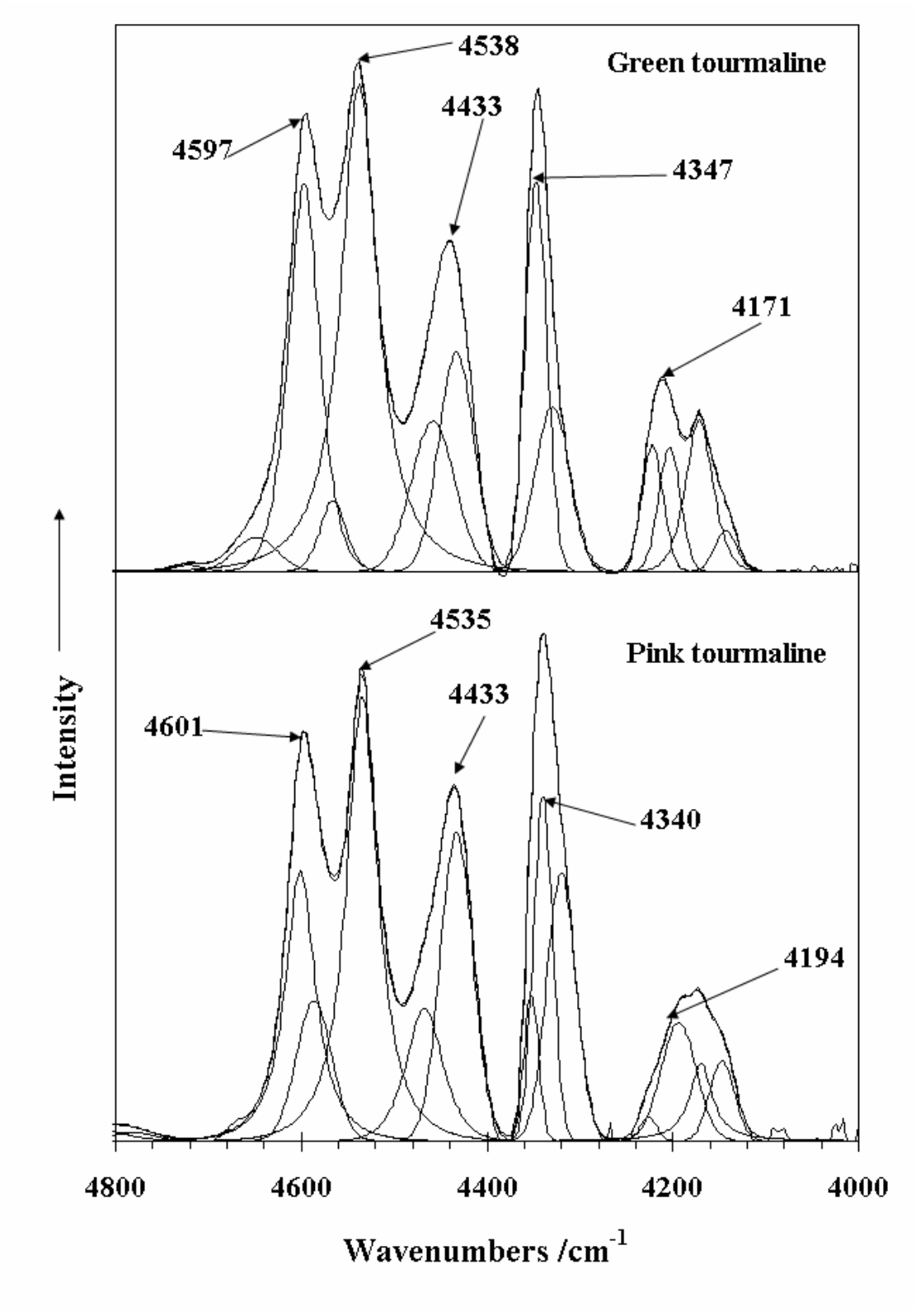
4538
Green tourmaline
4433
4597
4347
4171
4535
Pink tourmaline
4433
4601
4340
4194
Intensity
4800
4600
4400
4200
4000
Wavenumbers /cm-1

Fig. 2c

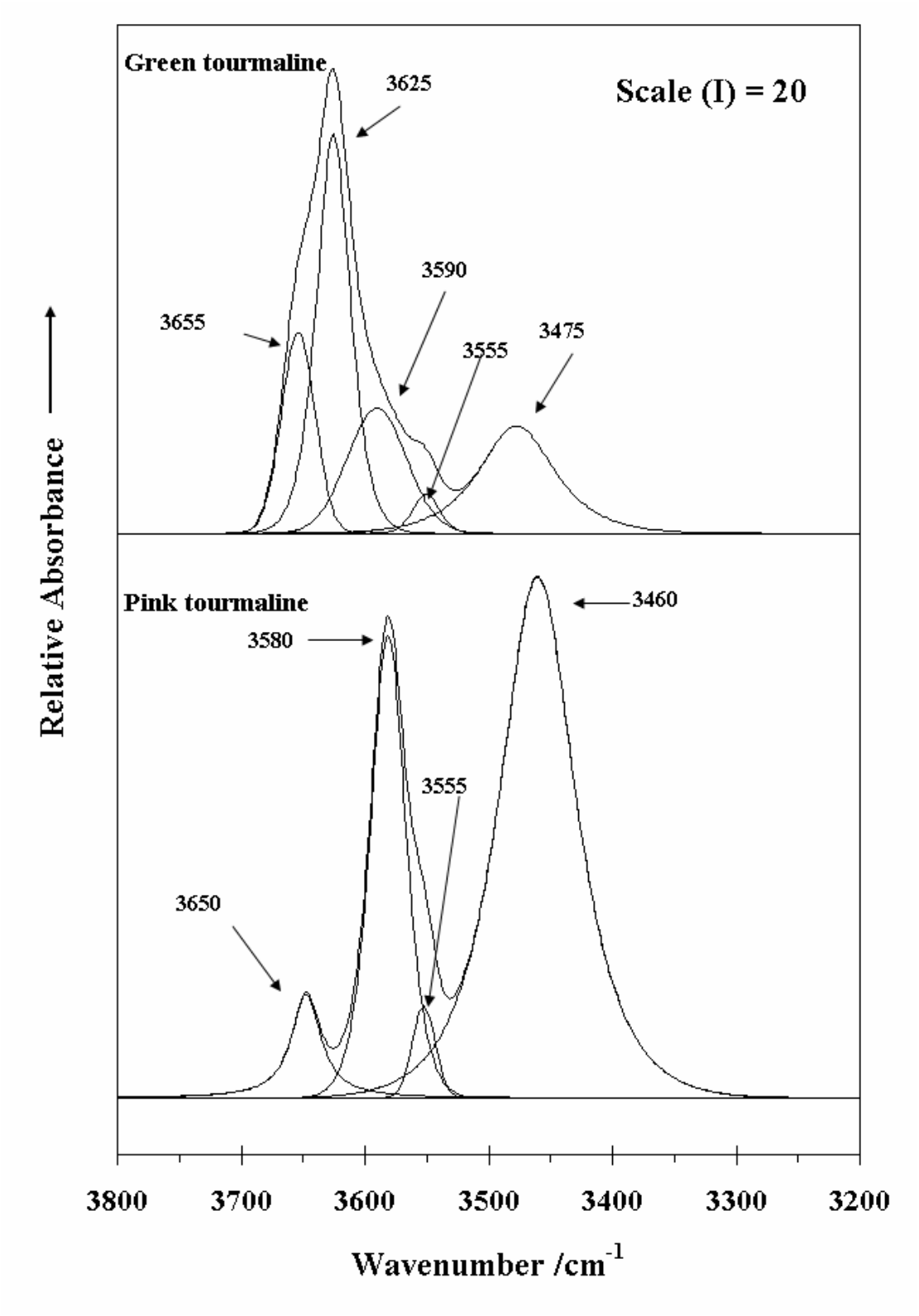
Green tourmaline
3625
Scale (I) = 20
3590
3655
3475
3555
Pink tourmaline
3460
3580
3555
3650
Relative Absorbance
3800
3700
3600
3500
3400
3300
3200
Wavenumber /cm-1

Fig. 3a

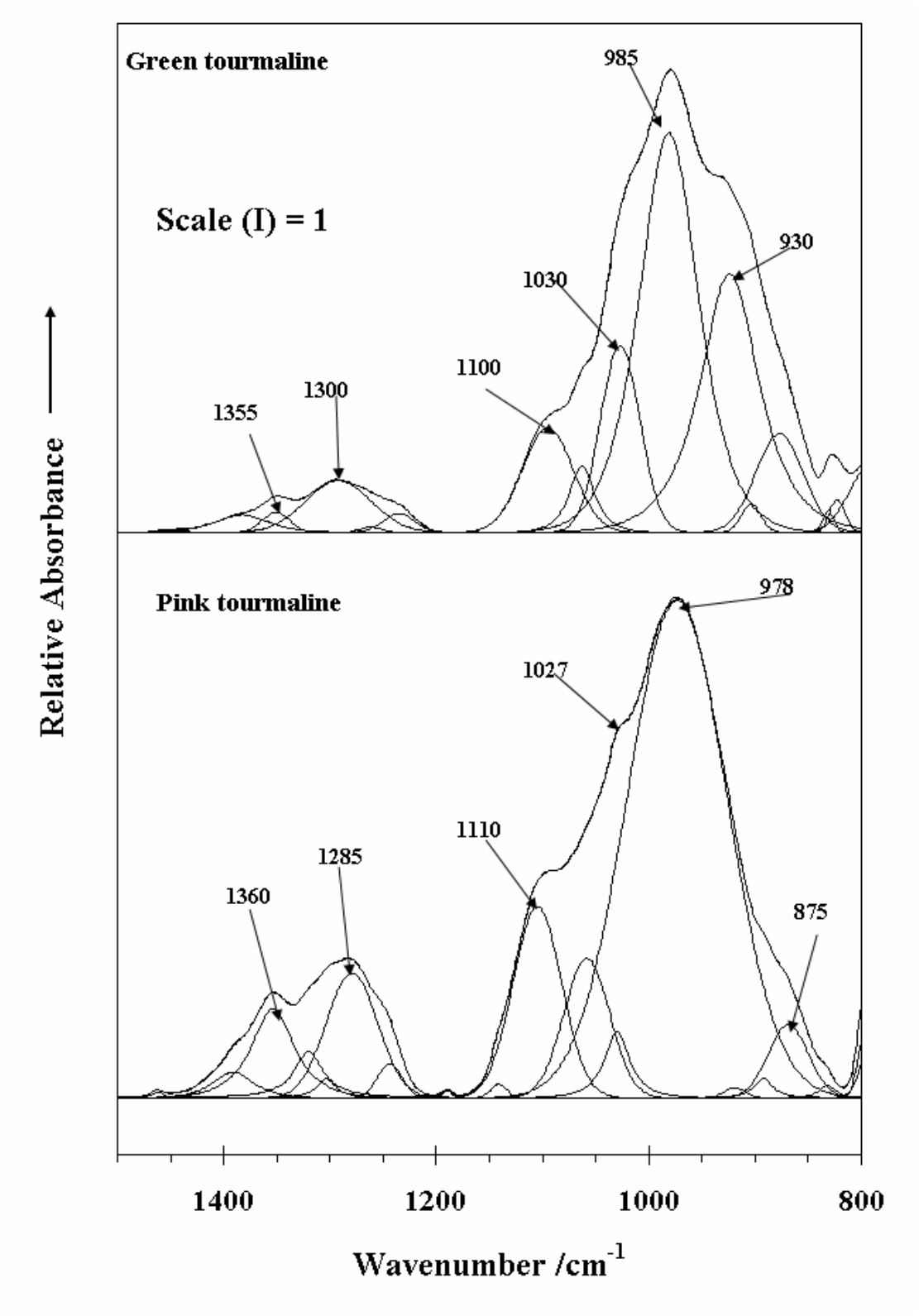
Green tourmaline
985
Scale (I) = 1
930
1030
1100
1300
1355
Pink tourmaline
978
1027
1110
1285
1360
875
Relative Absorbance
1400
1200
1000
800
Wavenumber /cm-1

Fig. 3b

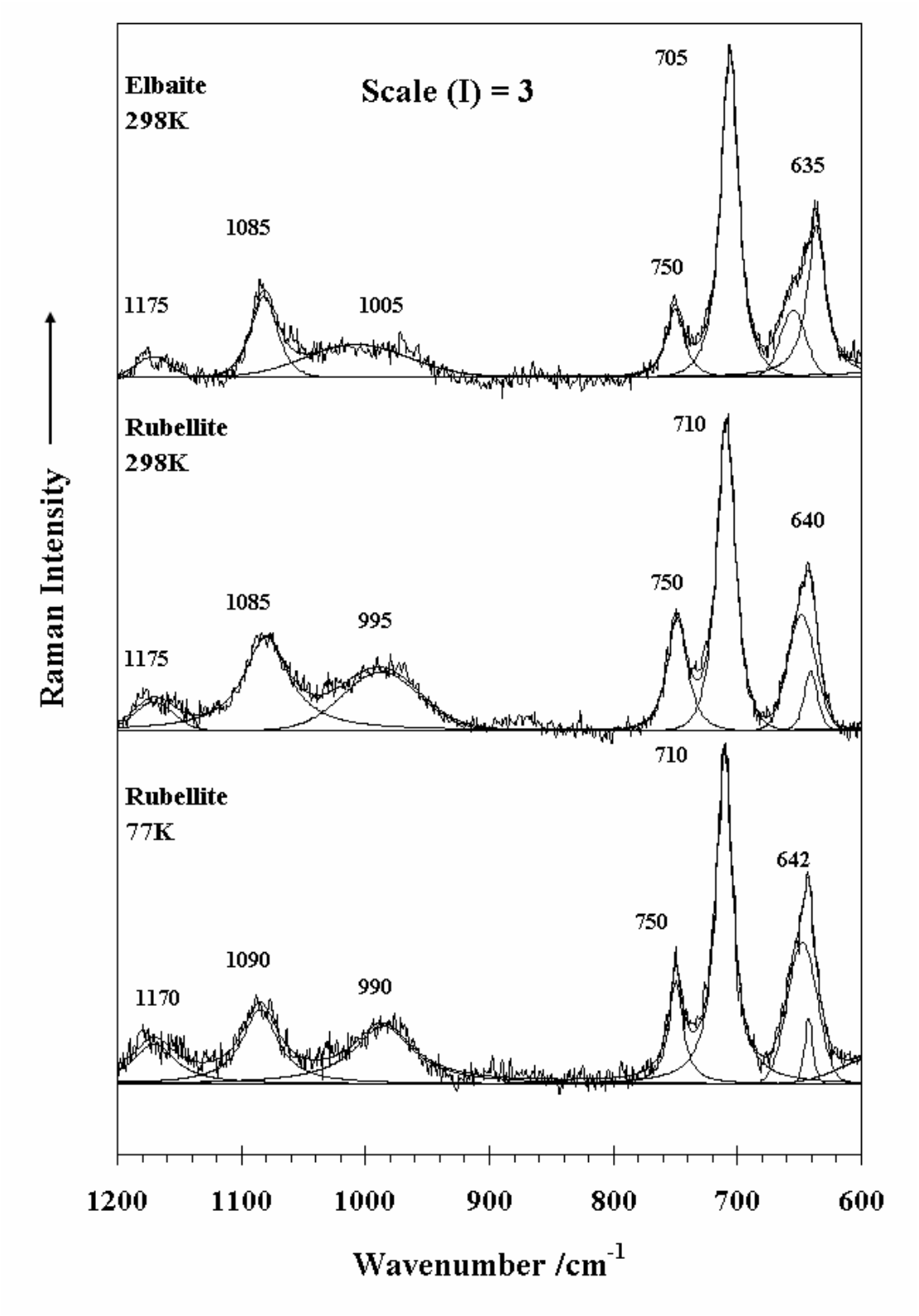
Elbaite
298K
Scale (I) = 3
705
635
1085
750
1175
1005
Rubellite
298K
710
640
750
1085
995
1175
Rubellite
77K
710
642
750
1090
990
1170
Raman Intensity
1200
1100
1000
900
800
700
600
Wavenumber /cm-1

Fig. 4a

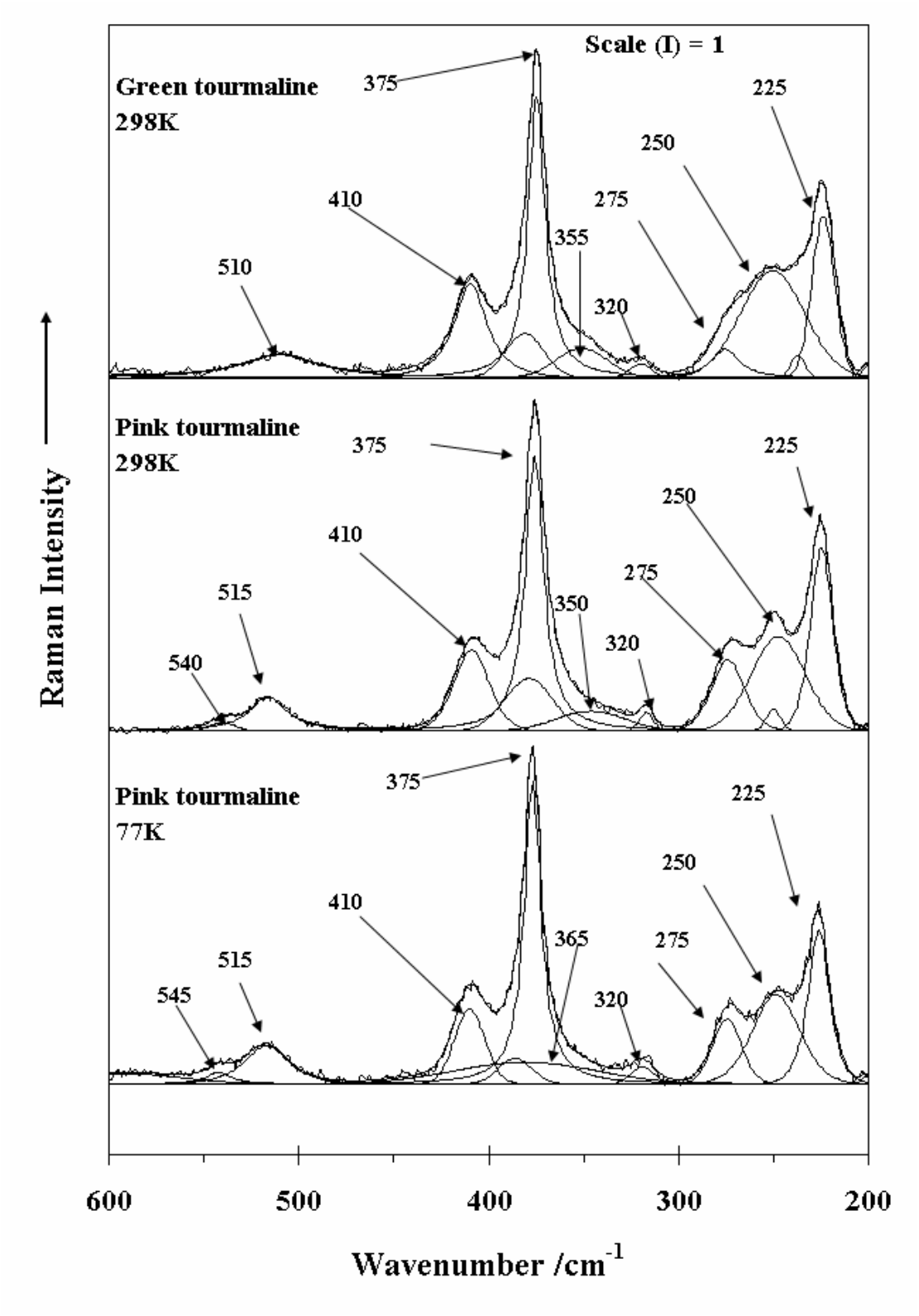
Scale (I) = 1
Green tourmaline
298K
375
225
250
410
275
355
510
320
Pink tourmaline
298K
375
225
250
410
275
515
350
320
540
Pink tourmaline
77K
375
225
250
410
365
275
515
545
320
Raman Intensity
600
500
400
300
200
Wavenumber /cm-1

Fig. 4b